

Structure, solution chemistry, antiproliferative actions and protein binding properties of non-conventional platinum(II) compounds with sulfur and phosphorus donors

SUPPORTING INFORMATION

Carolin Mügge,^{‡a} Claudia Rothenburger,^{‡a} Antje Beyer,^a Helmar Görls,^a Chiara Gabbiani,^b Angela Casini,^c Elena Michelucci,^d Ida Landini,^e Stefania Nobili,^e Enrico Mini,^e Luigi Messori,^{*b} Wolfgang Weigand^{*a}

[‡] These Authors contributed equally to this work.

^aInstitute of Inorganic and Analytical Chemistry, Friedrich-Schiller-University Jena, August-Bebel-Strasse 2, 07743 Jena, Germany, *Fax:* (+49) 3641 948102, *E-mail:* wolfgang.weigand@uni-jena.de

^b Laboratory of Metals in Medicine, Department of Chemistry, University of Florence, Via della Lastruccia 3, 50019 Sesto Fiorentino, Firenze, Italy, *Fax:* (+39) 055 4573385, *E-mail:* luigi.messori@unifi.it

^c Institut des Sciences et Ingénierie Chimiques, Ecole Polytechnique Fédérale de Lausanne (EPFL)CH-1015 Lausanne, Switzerland

^d Mass Spectrometry Center (CISM), University of Florence, Via U. Schiff 6, 50019 Sesto Fiorentino, Firenze, Italy

^e Department of Preclinical and Clinical Pharmacology, University of Florence, Viale Pieraccini 6, 50139 Firenze, Italy.

Table of Contents:

Figure S1. $^{31}\text{P}\{\text{H}\}$ NMR spectra of **7** and **8**.

Figure S2. Molecular Structures of **6**.

Figure S3. Molecular Structures of **7** and **8**.

Figure S4. Molecular Structures of **9** and **10**.

Table S1. Crystallographic data for compounds **6-10**.

Figure S5. Deconvoluted ESI-MS spectrum of **1**.

Figure S6. Deconvoluted ESI-MS spectrum of **2**.

Figure S7. Isotope pattern of the ESI-MS peak of **2** at charge State +8.

Figure S8. Isotope pattern of the ESI-MS peak of **3** at charge State +8.

Figure S9. Deconvoluted ESI-MS spectrum of **4** at charge State +8.

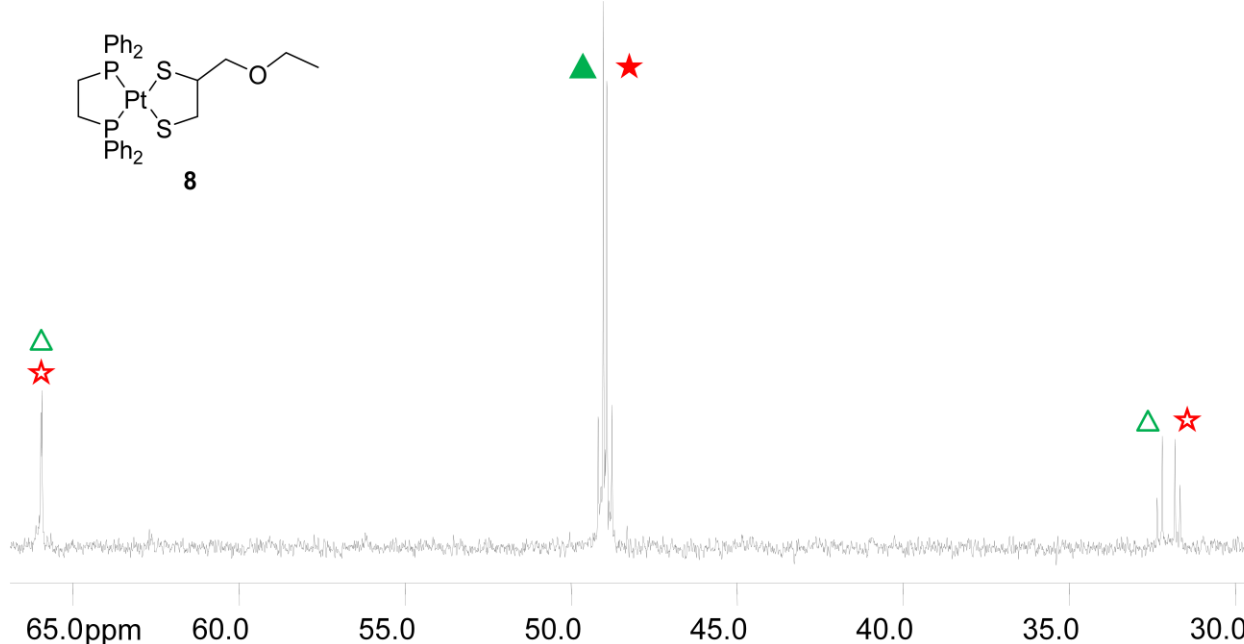
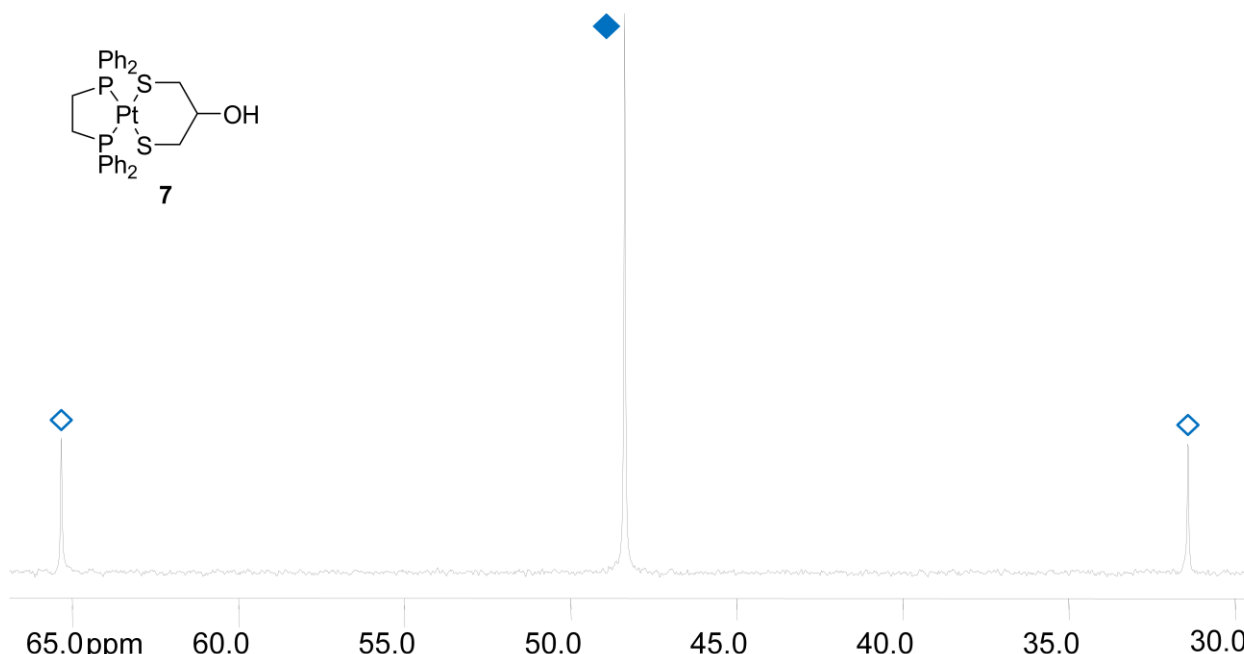


Figure S1. $^{31}\text{P}\{\text{H}\}$ NMR spectra (81 MHz, CDCl_3) of **7** (top) and **8** (bottom), showing the structural differences of both compounds. **7** is a symmetric complex leading to one singlet at $\delta = 48.4$ ppm (◆) with platinum satellites ($^1J_{\text{PPt}}$ 2748 Hz). **8**, bearing two different P atoms, gives a set of two doublets, each showing Pt satellites in an AB spin system. $\delta = 49.1$ ppm (▲, $^1J_{\text{PPt}}$ 2720 Hz, $^2J_{\text{PP}}$ 12 Hz), 48.8 ppm (★, $^1J_{\text{PPt}}$ 2778 Hz, $^2J_{\text{PP}}$ 12 Hz). Due to a strong roof effect, the satellite signals at 65.9 ppm appear merged to a pseudo-singlet.

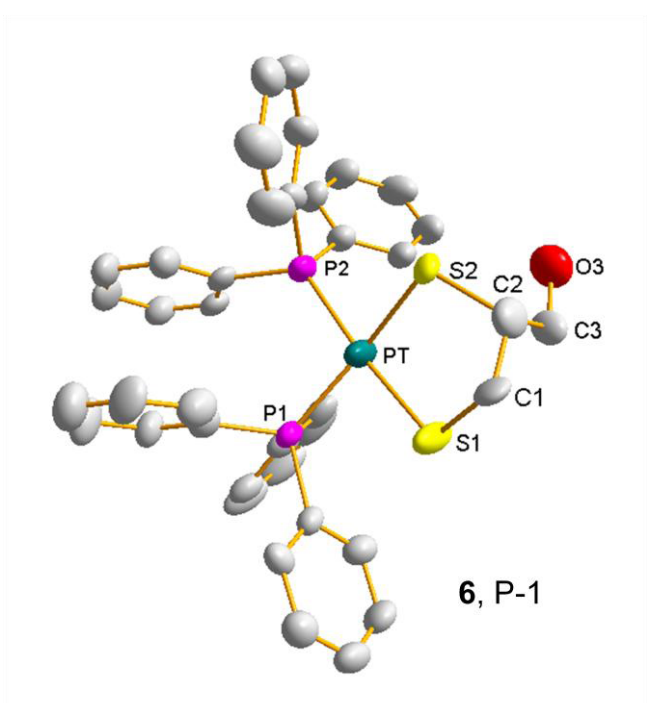


Figure S2. Molecular Structure of **6**. Disorders at the dithiolato moiety have been omitted for clarity.

Thermal ellipsoids are given at the 50 % probability level.

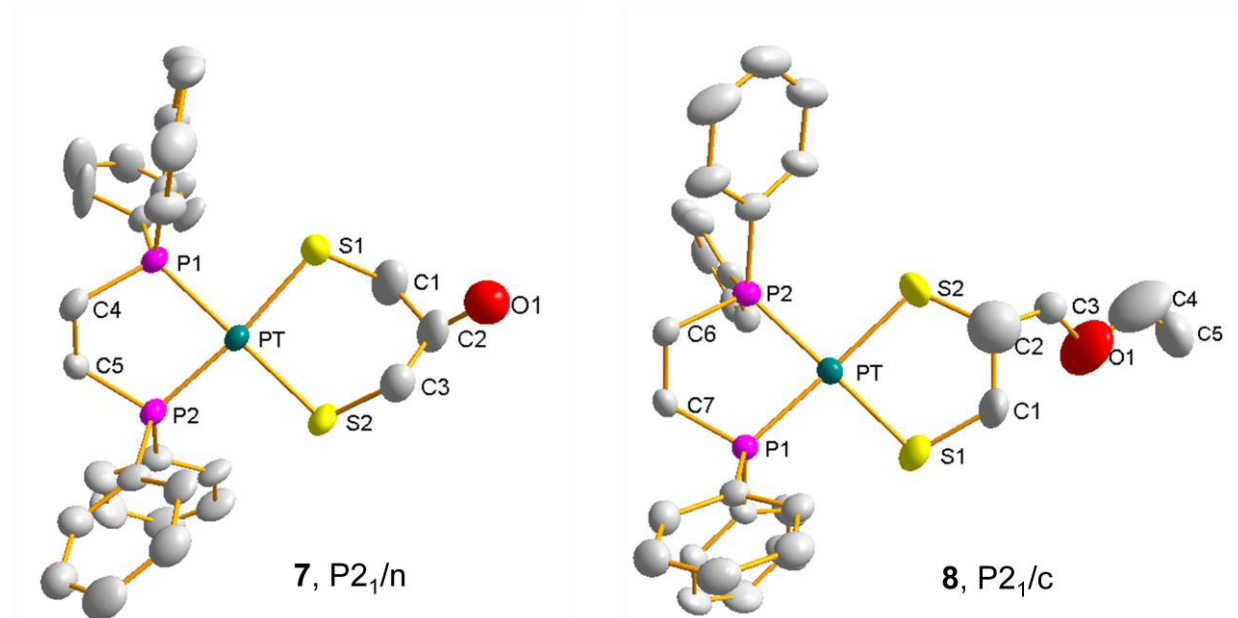


Figure S3. Molecular Structures of **7** and **8**. Disorders at the dithiolato moiety have been omitted for clarity. Thermal ellipsoids are given at the 50 % probability level.

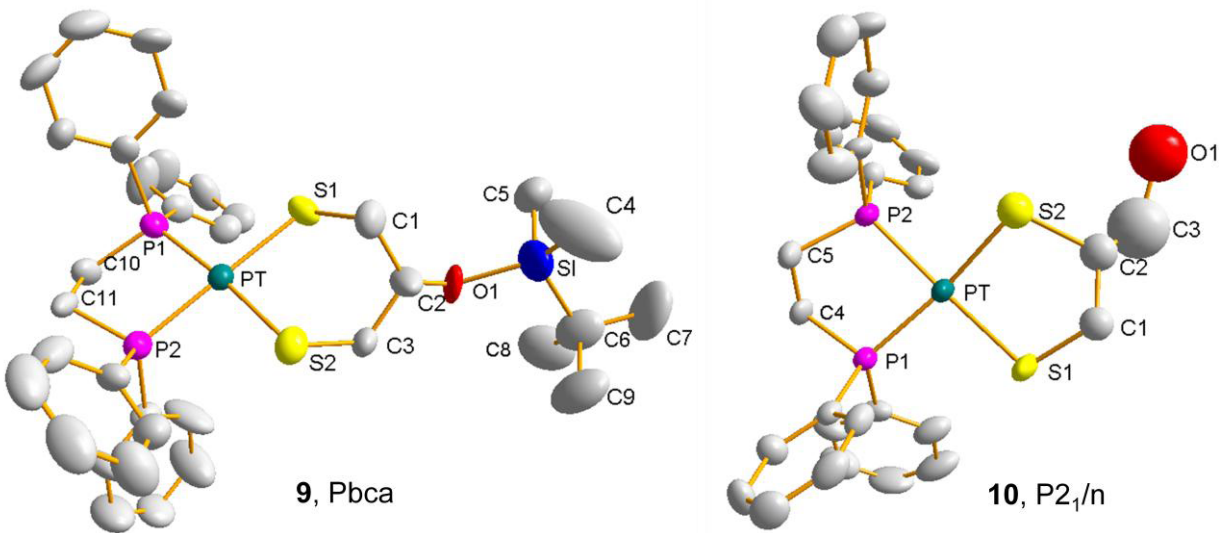


Figure S4. Molecular Structures of **9** and **10**. Disorders at the dithiolato moiety have been omitted for clarity. Thermal ellipsoids are given at the 50 % probability level.

Table S1. Crystal data and refinement details for the X-ray structure determinations of **6**, **7**, **8**, **9**, and **10**.

| Compound | 6 | 7 | 8 | 9 | 10 |
|--|---|---|--|--|--|
| formula | C ₃₉ H ₃₆ OP ₂ PtS ₂ , CHCl ₃ | C ₂₉ H ₃₀ OP ₂ PtS ₂ , CH ₄ O, H ₂ O | C ₃₁ H ₃₄ OP ₂ PtS ₂ | C ₃₅ H ₄₄ OP ₂ PtS ₂ | C ₂₉ H ₃₀ OP ₂ PtS ₂ |
| fw (g·mol ⁻¹) | 961.20 -90(2) | 749.72 -90(2) | 743.73 -90(2) | 829.94 -90(2) | 715.68 -90(2) |
| T/°C | | | | | |
| crystal system | triclinic | monoclinic | orthorhombic | monoclinic | monoclinic |
| space group | P $\bar{1}$ | P 2 ₁ /n | P 2 ₁ /c | P bca | P 2 ₁ /n |
| <i>a</i> /Å | 11.6368(13) | 9.0685(3) | 15.6013(6) | 17.8444(14) | 9.1382(3) |
| <i>b</i> /Å | 12.5618(13) | 28.1277(9) | 18.2591(7) | 13.7455(11) | 25.8648(9) |
| <i>c</i> /Å | 14.784(2) | 12.3952(3) | 10.9863(4) | 28.9636(18) | 12.1756(4) |
| <i>a</i> /° | 87.969(8) | 90 | 90 | 90 | 90 |
| β /° | 78.924(7) | 103.898(2) | 104.966(2) | 90 | 106.278(2) |
| γ /° | 64.993(4) | 90 | 90 | 90 | 90 |
| <i>V</i> /Å ³ | 1919.4(4) | 3069.16(16) | 3023.5(2) | 7104.2(9) | 2762.43(16) |
| <i>Z</i> | 2 | 4 | 4 | 8 | 4 |
| ρ (g·cm ⁻³) | 1.663 | 1.623 | 1.634 | 1.552 | 1.721 |
| μ (cm ⁻¹) | 40.88 | 48.39 | 49.08 | 42.18 | 53.68 |
| measured data | 12394 | 18527 | 20310 | 19282 | 15833 |
| data with I > 2σ(I) | 4729 | 4638 | 5116 | 3924 | 4081 |
| unique data (R _{int}) | 8227/0.0557 | 6922/0.0698 | 6808/0.0591 | 6757/0.1662 | 6188/0.0636 |
| wR ₂ (all data, on F ²) ^{a)} | 0.1753 | 0.1845 | 0.0979 | 0.2660 | 0.1598 |
| R ₁ (I > 2σ(I)) ^{a)} | 0.0894 | 0.0638 | 0.0386 | 0.0876 | 0.0569 |
| S ^{b)} | 1.126 | 1.014 | 1.007 | 1.018 | 1.023 |
| Res. dens./e·Å ⁻³ | 1.446/-1.670 | 2.860/-2.192 | 1.396/-1.953 | 2.655/-2.228 | 1.946/-1.788 |
| absorpt method | NONE | NONE | NONE | NONE | NONE |
| CCDC No. | 776102 | 776103 | 776104 | 776105 | 776106 |

^{a)} Definition of the *R* indices: R₁ = $(\sum ||| F_{\text{o}} | - F_{\text{c}} |||) \Sigma |F_{\text{o}}|$; wR₂ = $\{\Sigma [w(F_{\text{o}}^2 - F_{\text{c}}^2)^2] / \Sigma [w(F_{\text{o}}^2)]\}^{1/2}$ with $w^{-1} = \square^2(F_{\text{o}}^2) + (aP)^2 + bP$, P = $[2F_{\text{c}}^2 + \text{Max}(F_{\text{o}}^2)]/3$; ^{b)} s = $\{\Sigma [w(F_{\text{o}}^2 - F_{\text{c}}^2)^2] / (N_{\text{o}} - N_{\text{p}})\}^{1/2}$.

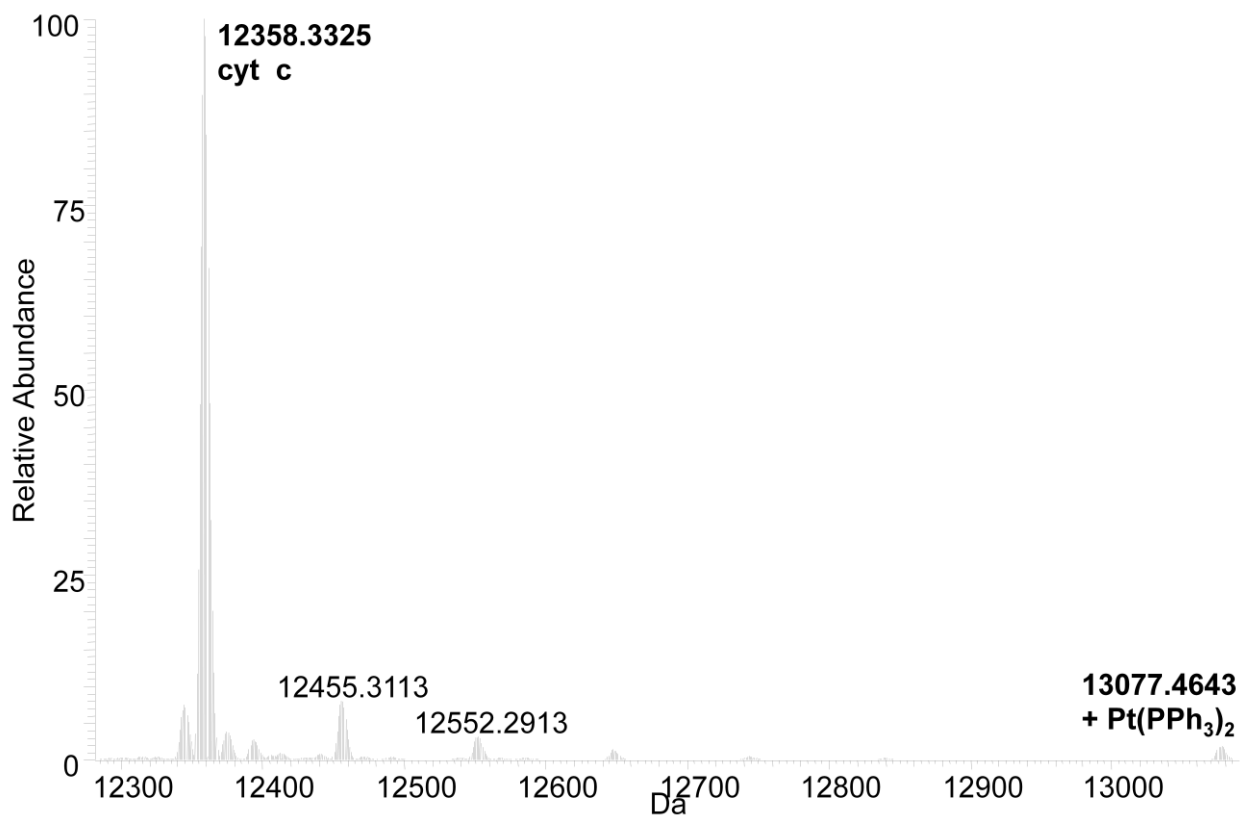


Figure S5. Deconvoluted ESI-MS spectrum of **1**, incubated with cyt c at a 1:3 ratio for 24 h at 37 °C.

A low-intensity signal (3 % r.i.) of a [cyt c + Pt(PPh₃)₂] fragment can be observed at 13077.46 Da.

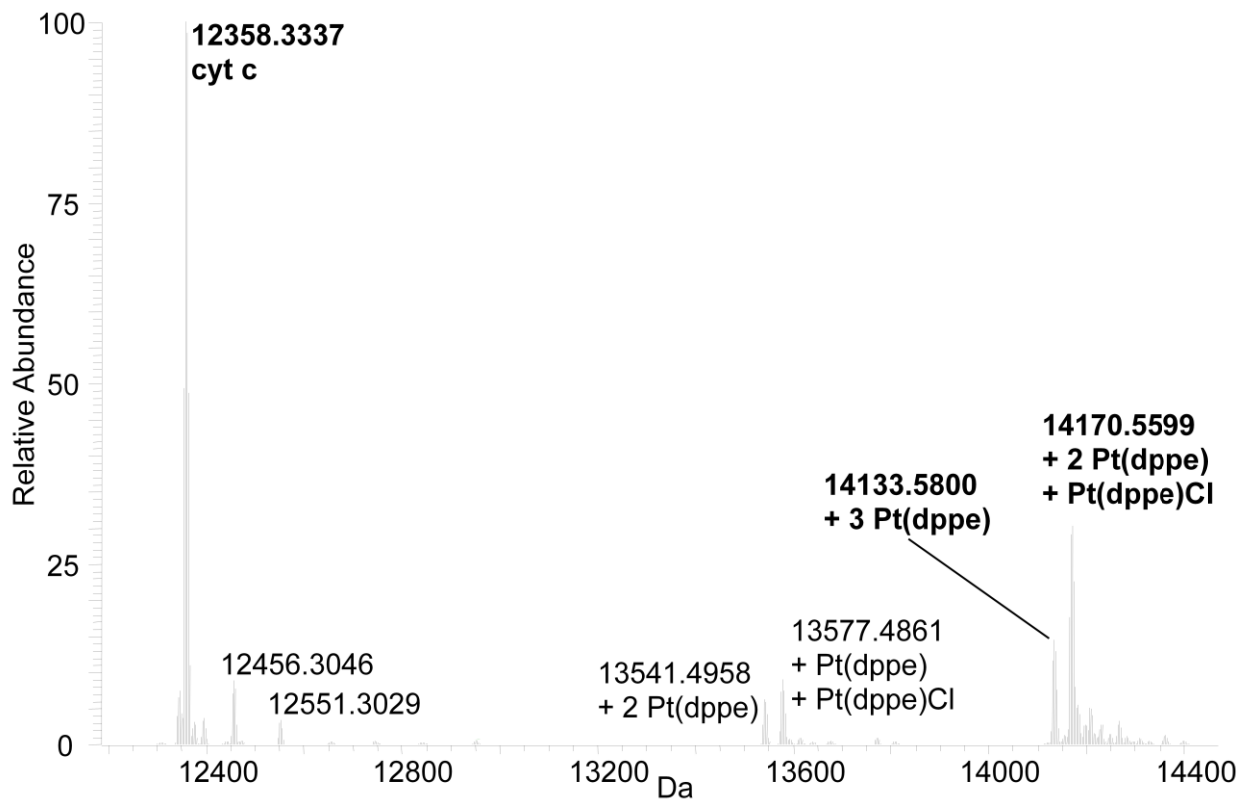


Figure S6. Deconvoluted ESI-MS spectrum of **2**, incubated with cyt c at a 3:1 ratio for 24 h at 37 °C.

Weak signals corresponding to 2 Pt(dppe) units and Pt(dppe) + Pt(dppe)Cl bound to cyt c are observed in the 13500-13600 Da range. The signal at 14233.6 Da, belonging to [cyt c + 3 Pt(dppe)] is weaker (15 % r.i.) than the one at 14170.6 Da ([cyt c + 2 Pt(dppe) + Pt(dppe)Cl], 30 % r.i.).

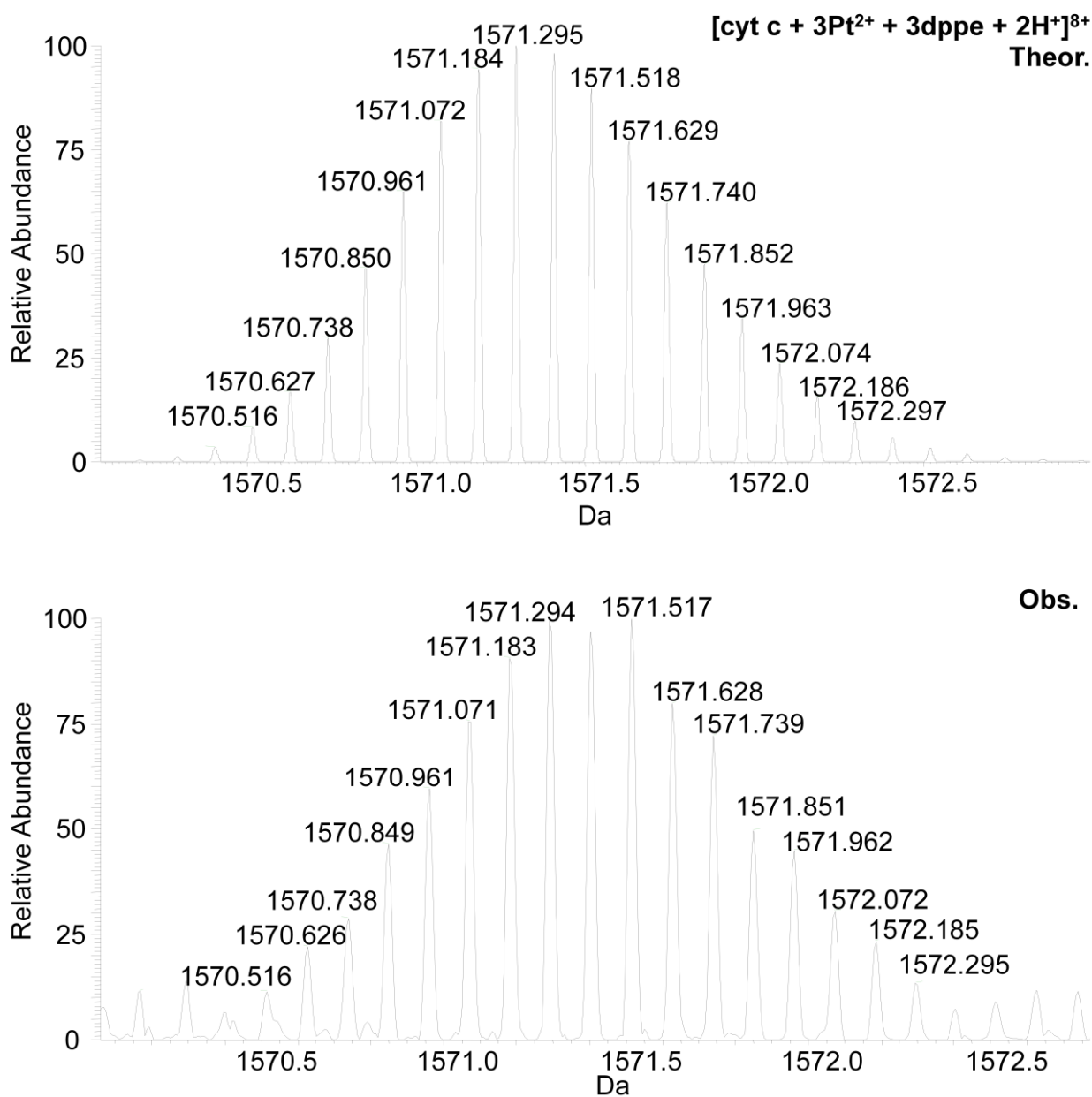


Figure S7. Isotope pattern of the ESI-MS peak of **2**, assigned to cyt c with 3 $[\text{Pt}(\text{dppe})]^{2+}$ fragments at $Z = +8$. Top, theoretical pattern; bottom, observed signal.

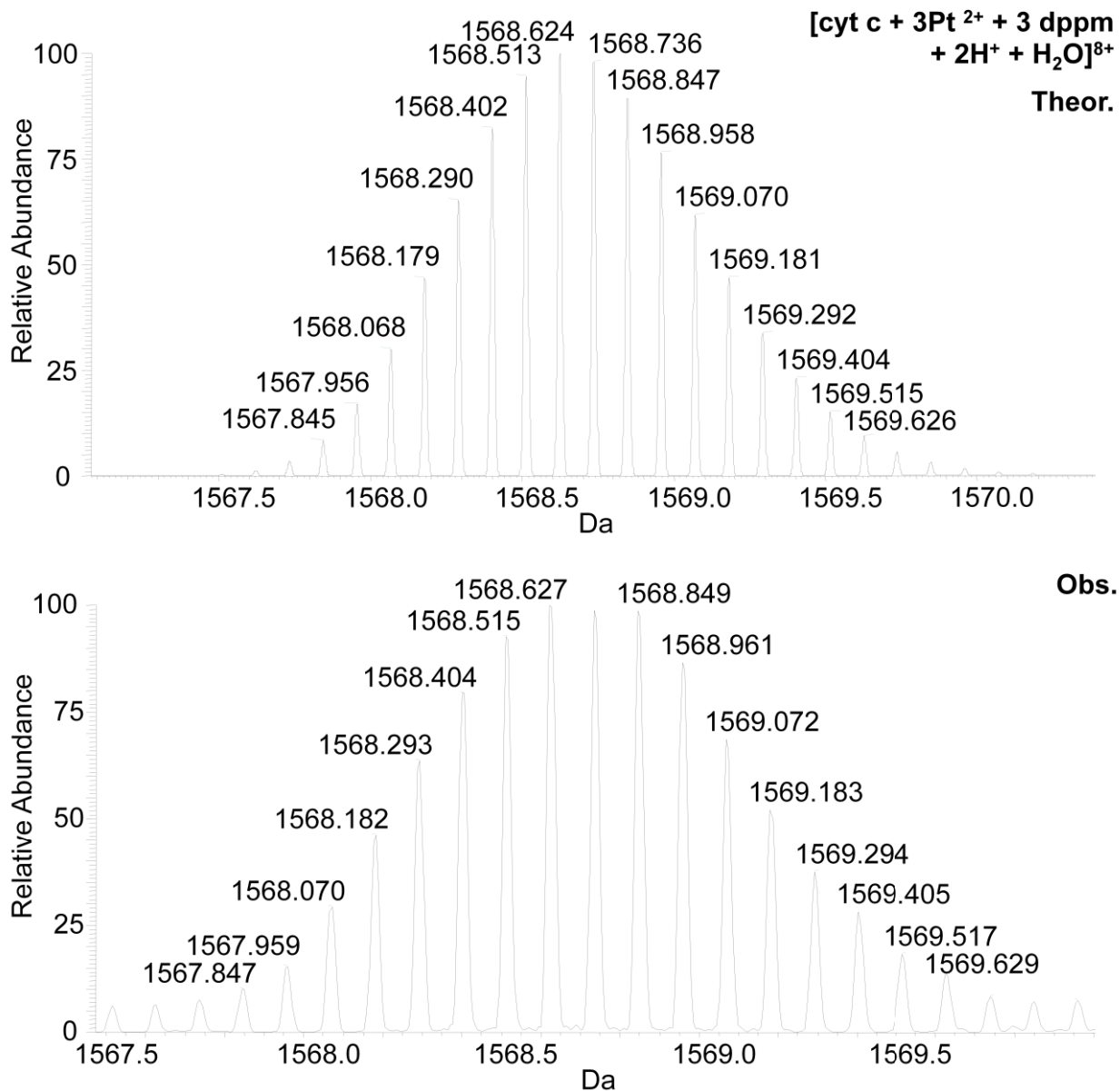


Figure S8. Isotope pattern of the ESI-MS peak of **3**, assigned to cyt c with 2 Pt(dppm) and 1 $[\text{Pt}(\text{dppm})\text{H}_2\text{O}]^{2+}$ bound fragments at $Z = +8$. Top, theoretical pattern; bottom, observed signal.

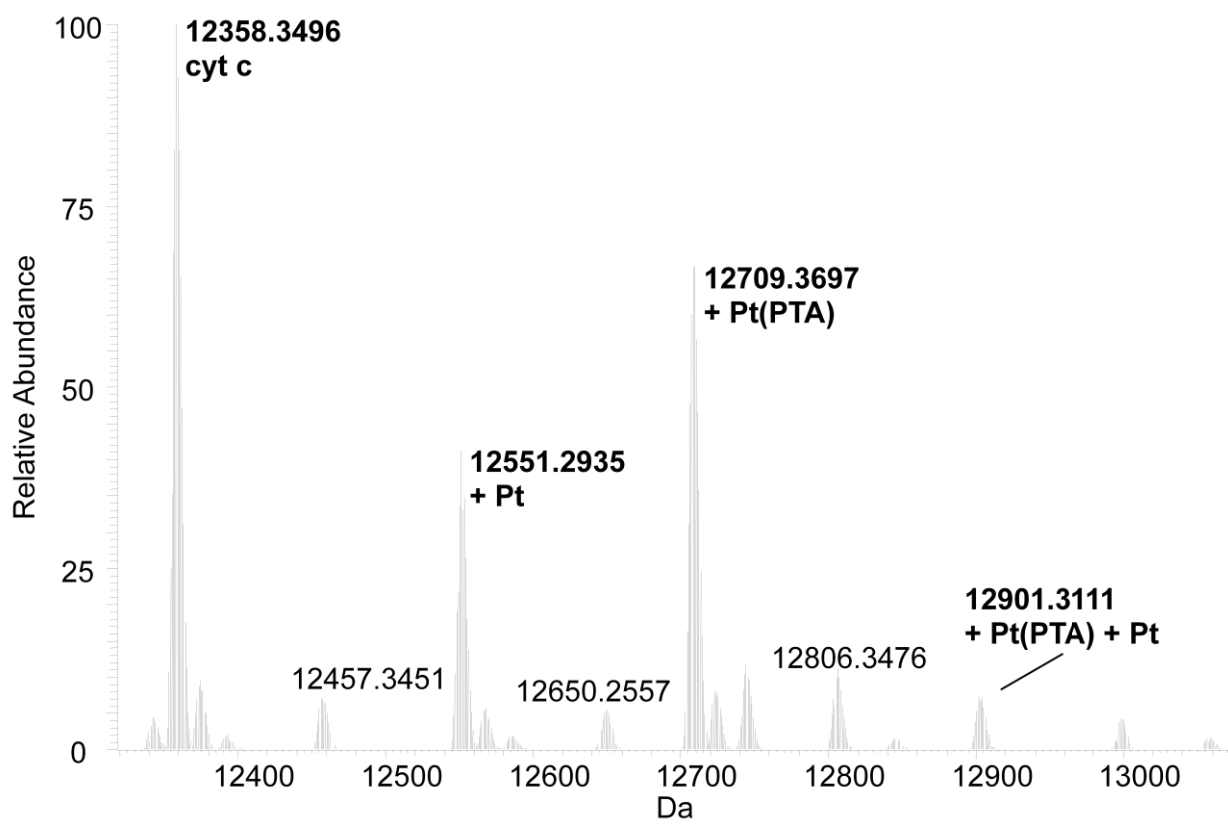


Figure S9. Deconvoluted ESI-MS spectrum of **4**, incubated with cyt c at a 1:1 ratio for 96 h at 37 °C.

Various adducts can be observed and progressive loss of the PTA ligands is indicated.